PERGAMON

International Journal of Multiphase Flow 26 (2000) 503–516

International Journal of Multiphase Flow

www.elsevier.com/locate/ijmulflow

Ellipsoidal bubble diffusion in a turbulent shear layer

B. Ford, E. Loth*

Department of Aeronautical and Astronautical Engineering, 306 Talbot Laboratory, 104 South Wright Street, University of Illinois at Urbana-Champaign, Urbana, IL 61801-2935, USA

Received 26 March 1998; received in revised form 12 April 1999

Abstract

The objective of this research was to document the relative diffusion widths of ellipsoidal air bubbles in water at very low void fraction for a turbulent mixing layer. This was accomplished by recording the transverse concentration distribution of bubbles in an upward-flowing two-stream, turbulent, planar free shear layer of tap water. Ellipsoidal air bubbles with nominal equivalent diameters of 2.5, 3.5 and 4.5 mm were injected directly into the shear layer and illuminated by a scanning laser beam 12–36 cm downstream. For each test condition, three image intensity distributions (based on long-time exposures which resolved individual bubbles in the shear layer) were recorded. From the digitized images, the average Gaussian dispersion widths of the bubble concentration distributions were measured for three bubble sizes, two shear layer speeds, and six streamwise locations. The results demonstrate increased bubble concentration width at larger bubble sizes and at higher flow speeds. The former is primarily attributed to the interaction between turbulent diffusion and the deformation-induced trajectory oscillations (inherent to rising ellipsoidal bubbles) while the latter is attributed to the increased ratio of fluid turbulent velocity fluctuations to bubble terminal velocity. © 2000 Elsevier Science Ltd. All rights reserved.

Keywords: Free shear layer; Diffusion; Bubbles; Ellipsoidal

1. Introduction

The turbulent diffusion of ellipsoidal bubbles has often been examined in the context of wall-bounded flows, notably pipe flows (e.g., Serizawa et al., 1975). While there have been several

* Corresponding author. Tel.: +1-217-244-5581; fax: +1-217-244-0720.
E-mail address: e-loth@uiuc.edu (E. Loth).

PII: S0301-9322(99)00026-9

recent characterizations of the turbulent dispersion of bubbles in free shear layers, such studies have primarily been based on numerical simulations and for non-deformable (spherical) bubbles (e.g., Tio et al., 1993; Stewart and Crowe, 1993; Sene et al., 1994). Loth (1997) focused on three important non-dimensional parameters for turbulent dispersion in a bubbly flow: the local Stokes number, the eddy Froude number, and the relative turbulence intensity. These three parameters are defined in the following and are consistent with the dimensionless parameters of Tio et al. (1993), Sene et al. (1994), and Stock (1996). The local Stokes number (St_Λ) is the ratio of bubble response time to local eddy lifetime and is given as:

$$St_\Lambda = \frac{\tau_B}{\tau_\Lambda} \tag{1}$$

where the local eddy time scale is defined as a characteristic integral length (Λ) divided by a characteristic eddy velocity in the direction of diffusion being considered, such that for transverse diffusion,

$$\tau_\Lambda = \frac{\Lambda}{v'_{rms}} \tag{2}$$

where v'_{rms} is the transverse velocity fluctuations. The response time for air bubbles in a liquid can be approximated as

$$\tau_B = \frac{4C_M d_B}{3V_{term}C_D} \tag{3}$$

where C_M is the added mass coefficient, d_B is the bubble volume-equivalent diameter, V_{term} is the bubble terminal (relative) velocity, and C_D is the coefficient of drag acting on the bubble. Note, recent results by Ford and Loth (1998) indicate that while conventional drag coefficient expressions are not appropriate for describing the instantaneous force on ellipsoidal bubbles in turbulent flow, the use of a terminal drag coefficient is reasonable for describing the mean drag.

The second non-dimensional parameter mentioned by Loth (1997) is the ratio of hydrodynamic and hydrostatic pressure gradients, i.e. the local eddy Froude number, herein defined as

$$Fr_\Lambda \equiv \frac{\left(v'_{rms}\right)^2}{4g\Lambda} \tag{4}$$

where g is the magnitude of gravitational acceleration. Note the local Stokes number and local eddy Froude number are related by the third non-dimensional diffusion parameter, the relative turbulence intensity (ζ), which is the ratio of the local fluid turbulent velocity to the bubble terminal velocity, i.e.:

$$\zeta \equiv \frac{v'_{rms}}{V_{term}} = \frac{3C_D\Lambda St_\Lambda}{4C_M d_B}. \tag{5}$$

Note that ζ indicates the nature of bubble-eddy interaction timescale, i.e. if $\zeta \gg 1$ interactions

are dominated by eddy lifetime, but if $\zeta \ll 1$ interactions are dominated by the crossing trajectory effect (Stock, 1996; Loth, 1997). Of these three parameters (St_Λ,Fr_Λ,ζ) two are independent (Loth, 1997) and thus should be considered when interpreting trends. (Note some previous studies discuss trends in Stokes number without specification of whether Froude number or relative turbulent intensity is held constant, which can provide two different results.)

The above parameters are used to characterize the large-scale eddy influence on the *temporal* diffusion rates of bubbles with respect to that of a scalar. The *spatial* diffusion rates of bubbles need to be considered (with respect to that of a scalar) for the case where a non-zero component of gravity is in the direction of mean flow convection. In this context, Loth (1997) also mentioned the importance of a fourth parameter, which is simply the ratio of mean fluid convection speed (U_{mean}) to the component of bubble terminal velocity (V_{term}) in the direction of mean flow convection. This parameter allows us to relate (in an approximate fashion) the temporal diffusion rate to the spatial diffusion rate, since the latter is shifted by a mean drift bias. For the example of bubbles in an upward flowing shear layer, increasing the relative bubble velocity for a constant mean fluid convection speed will result in a reduced spatial transverse diffusion rate for an equal temporal diffusion rate, i.e. a mean drift bias toward smaller spatial diffusion.

The above parameters can help describe the following studies. Numerical bubble dispersion in an array of Stuart vortices with gravity oriented perpendicular to the streamwise direction and with bubbles modeled as rigid spherical buoyant particles was studied by Tio et al. (1993). The results indicated the importance of the ratio of Stokes number to eddy Froude number, in that typically bubbles escape for values of this ratio greater than a constant and are trapped for values of this ratio less than a constant. Similar numerical studies in Stuart vortices were conducted by Stewart and Crowe (1993), although these were only conducted for a fixed eddy Froude number. Sene et al. (1994) numerically examined bubble transport in a turbulent shear flow modeled by a discrete vortex method, and also noted sensitivity to Froude number. Loth (1997) used a simple theoretical model to examine Stokesian bubble diffusion and showed that the independent influences of St_Λ and Fr_Λ on the diffusion ratio can both be profound.

There has been little experimental documentation of ellipsoidal bubble diffusion rates in free shear flows in the limit of no bubble–bubble interaction and no flow modulation (i.e. no change in the mean liquid characteristics due to the bubble presence). It should be noted that these two limits require void fractions much less than 1% as described by Loth and Cebrzynski (1995) and Elgobashi (1994). The combination of a canonical turbulent free shear layer and ellipsoidal bubbles at very low void fraction is the condition for the present study.

The fact that the bubbles considered herein are deformable suggests other relevant previous studies. Clift et al. (1978) noted that as bubbles become large enough to deform (>1.2 mm in diameter), their geometry becomes ellipsoidal with the minor axis approximately in the direction of gravity. The degree of deformity is often related to the bubble Weber number, which is controlled by two dimensionless surface tension groups: the Morton number (independent of bubble size) and the Bond number. The Bond number (B) is defined as

$$B = \frac{\rho g d_{\text{B}}^2}{\sigma} \tag{6}$$

where ρ is the density of the fluid surrounding the bubble and σ is the surface tension of the

gas–fluid interface. In addition, for sufficiently high Reynolds numbers (as are found for air bubbles in water), the trajectory in quiescent conditions becomes helical or sinusoidal, and the terminal velocity may decrease with bubble diameter due to the added energy consumed by this unsteady motion. Ford and Loth (1998) found that this inherent deformation-induced motion is qualitatively preserved to a great extent in turbulent flow and indeed dominates the transverse side forces for relative turbulence intensities of the order of one-tenth (as are considered herein). This observation is generally consistent with earlier work done by Serizawa et al. (1975). However, the quantitative effect of the deformation-induced motion on turbulent diffusion of ellipsoidal bubbles in a free shear flow has not been previously considered.

2. Experimental

The present experimental study was conducted in a closed-loop water tunnel with a vertical upward-flowing test section. The tunnel has a total recirculation length of about 20 m and a 9:1 contraction ratio just upstream of the test section and just downstream of a set of rectangular grid flow conditioners. The test section is approximately 1 m long with interior cross-section dimensions of 0.3 m by 0.3 m. Optical access is available on all sides through four removable Plexiglas windows with a thickness of 28.6 mm. The tunnel volume is approximately 4500 l, with a passive bubble trap located at the top of the water tunnel to eliminate bubble recirculation. The tap water in the tunnel was filtered through filter papers with a 2.5 μm pore size. No other water treatment was employed, such that immobilization of the liquid–gas interface caused by natural contaminants is expected to be consistent with other 'tap water' experiments.

The unforced free shear layer is created by a splitter plate with pressure-correcting screens (discussed by Loth and Cebrzynski, 1995). Two tunnel speed settings were used for the current shear layer research. The baseline setting corresponded to a high-side velocity of 42.5 cm/s and a velocity ratio of 0.23, yielding an average liquid velocity (U_{mean}) of 26 cm/s. A second setting of the tunnel yielded a high-side velocity of 95.5 cm/s and a velocity ratio of 0.37 ($U_{\text{mean}} = 65.0$ cm/s). The baseline speed setting results in a high Reynolds number of 26,000 based on the thickness of the shear layer, which yields a fully developed turbulent flow (Oakley et al., 1996). Further details of the experimental apparatus can be found in Ford (1997).

Compressed air was delivered to various circular stainless steel injector tips in order to create mono-disperse bubbles with nominal equivalent bubble diameters of 2.5, 3.5 and 4.5 mm at a rate of approximately 10 Hz. The resulting void fraction is very low (Oakley et al., 1996). The optical method for determining the actual equivalent diameters of the ellipsoidal bubbles within the shear layer used the bubble's dual reflection properties and produced a maximum diameter uncertainty of 8% (Ford and Loth, 1998). Two separate injector exit streamwise positions were used in the current research: 12 and 24 cm below the camera field of view (which itself was fixed in all tests). In both cases, the bubble injector was located at the same transverse location as the shear layer splitter tip. Since ellipsoidal air bubbles in water achieve their terminal velocity in less than a centimeter, the injector locations assured that the bubble motion in the field of view was essentially independent of their formation at the injector. In addition, the

wake of the thin 1.6 mm diameter injector tube is expected to have a negligible impact on the downstream shear layer development and structure.

The field of view of the test section was illuminated by a 5 W argon-ion laser, which was coupled with a 24-sided rotating polygonal mirror and a 145 mm diameter collimating lens (Fig. 1). Various other lenses and mirrors were included for beam focusing and steering. The polygonal mirror rotated at 8.0 Hz, such that the laser beam was swept through the field of view 192 times per second to 'stroboscopically' illuminate the bubbles in the field of view. A Nikon 35 mm camera was used to record bubble images on TMAX 400 film using long exposure photography (30 s). The long exposure time was chosen as it allowed a statistically large number of bubbles in each image (approximately 1800), yet individual bubbles could still be observed. The first point is illustrated in Fig. 2, which shows a high resolution scan of a sample long-exposure photograph of the test section field of view (12.2 cm high and 19.2 cm wide). The flow is upwards and contains nominal 4.5 mm bubbles which can be seen to obey an approximately Gaussian variation in number density along the transverse direction. A sample 7×7 mm portion of the field of view is marked with a box on Fig. 2, and is also magnified by a factor of 25 in Fig. 3 such that individual bubbles may be observed. Here we can see also two overlapping bubbles in the upper right-hand corner of the image. However, despite the high bubble concentration and even at the largest bubble size, only a small fraction (less than 4% on average) of overlap for the total bubble image area is observed. In this manner, three images for each bubble size, injector position, and tunnel speed were recorded.

The film negatives of the bubble images were digitized using a high resolution digital scanner (600 ppi). After digitization, each image was cut into three spanwise strips (e.g., see horizontal lines in Fig. 2), so that the bubble dispersion concentration could be measured at three discrete distances from the injector tip for each of the two bubble injector exit positions. Each of these spanwise strips was 40.7 mm long in the streamwise direction. For each test condition, three

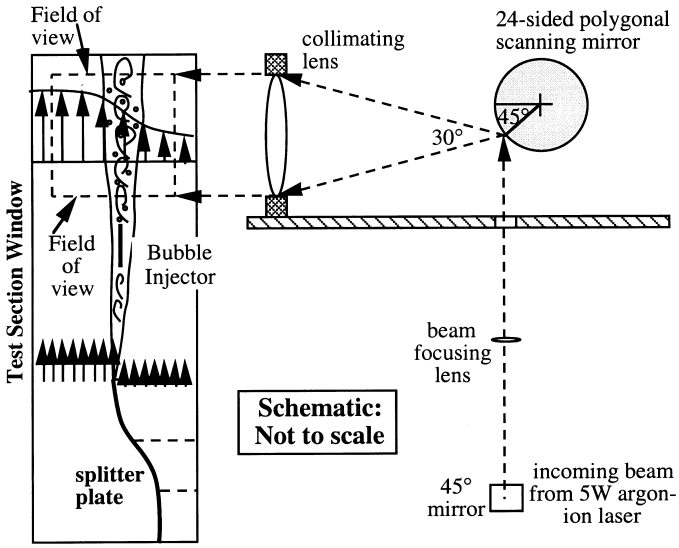

Fig. 1. Experimental schematic and optics arrangement with respect to the field of view.

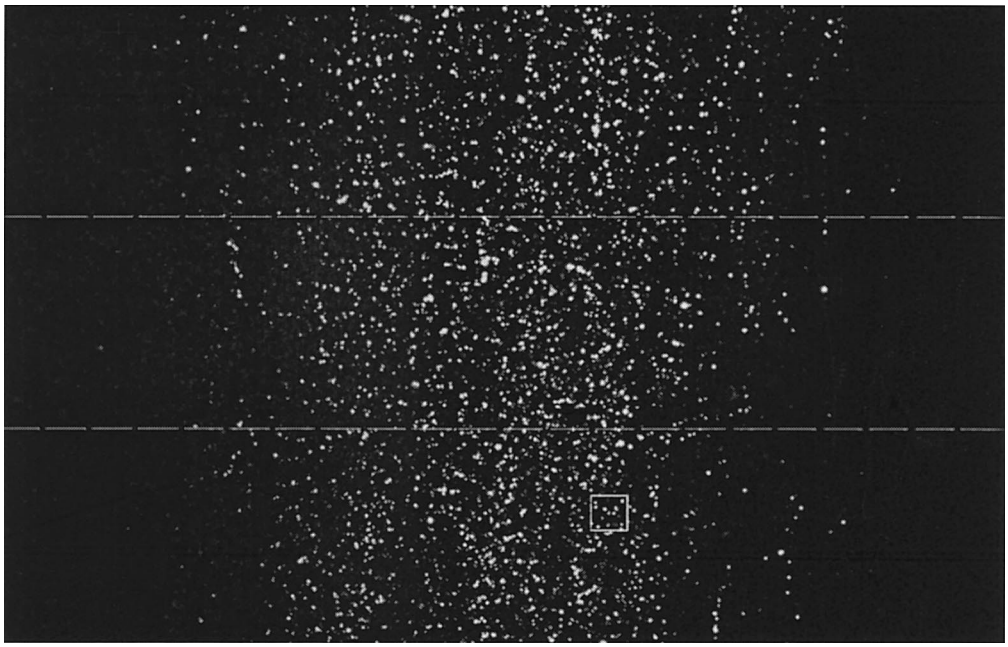

Fig. 2. Digitized image of a sample thirty-second exposure of the 4.5 mm bubbles in the turbulent shear layer.

separate digital intensities distributions (from separate photographs) were averaged together for all the spanwise strips (to increase the signal-to-noise ratio while avoiding increases in bubble image overlap). Finally, each of these averaged spanwise strips were averaged over the streamwise direction to yield a transverse intensity distribution within that discrete region of the test section. The resulting image intensity distributions were not artificially smoothed in any manner. The result allows us to approximate the spatially-averaged void-fraction concentration as linearly proportional to the summation of image intensity over a given area of the field of view. This proportionality was validated by measuring the average recorded intensity per bubble for fixed regions from image to image (i.e. at separate times) whereby deviations in integrated image intensity of 3% or less were found for groups of one-hundred bubbles.

Since all the resulting transverse intensity distributions were nearly Gaussian in shape (similar to results by Serizawa et al., 1975), a Gaussian curve fit was used to represent the experimental distribution. The curve fit was determined by minimizing the rms deviation from the experimental distribution (at approximately 400 transverse locations). As a typical example, Fig. 4 shows the experimental and Gaussian distributions versus the transverse coordinate for the low-speed flow 2.5 mm bubble case. The results shown in Fig. 4 were very typical of all results (i.e. nearly symmetric and of Gaussian shape). The distributions were centered on the transverse injection location (and on the splitter plate transverse location) to within 2–3 mm. To quantify the local concentration width of the bubble distribution, we define a bubble distribution thickness (δ_{bub}) as the width of the Gaussian curve fit within which the bubble concentration is 10% or more of the maximum concentration (see Fig. 4). As such, a

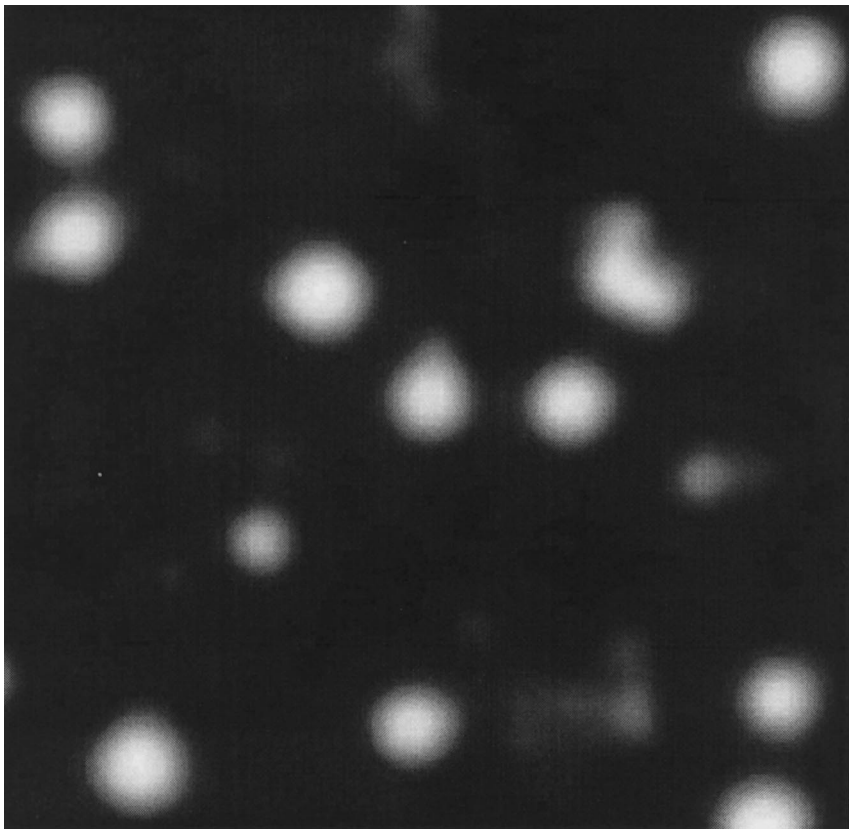

Fig. 3. Close-up of the boxed area of Fig. 2 showing individual bubbles and an overlapping pair in upper right-hand corner.

concentration width was obtained at six streamwise locations for each bubble size and flow speed.

The uncertainty of δ_{bub}, was estimated to be 7% or less by taking into account errors associated with overlapping bubbles, laser attenuation, and finite bubble populations. The bubble concentration thickness was then normalized by δ_{vel}, the 5–95% velocity thickness (Oakley et al., 1996). In the current experiment, bubbles are moving in and out of the plane of measurement, but the injection point is centered on the measurement plane and there are no mean variations of the liquid turbulence statistics or of the liquid mean velocity normal to the plane. In addition, the majority of the injected bubbles were captured within the laser sheet (whose effective bubble imaging thickness is about 1 cm). The transverse spread of the measured distribution will thus be qualitatively consistent with that of a line-source. However, the out-of-plane diffusion will reduce the net void fraction captured in the plane and thus reduce the magnitude of the void fraction peak. As such, the relative change in the *normalized* distribution thickness of the void profiles will be the primary objective measurement of these tests.

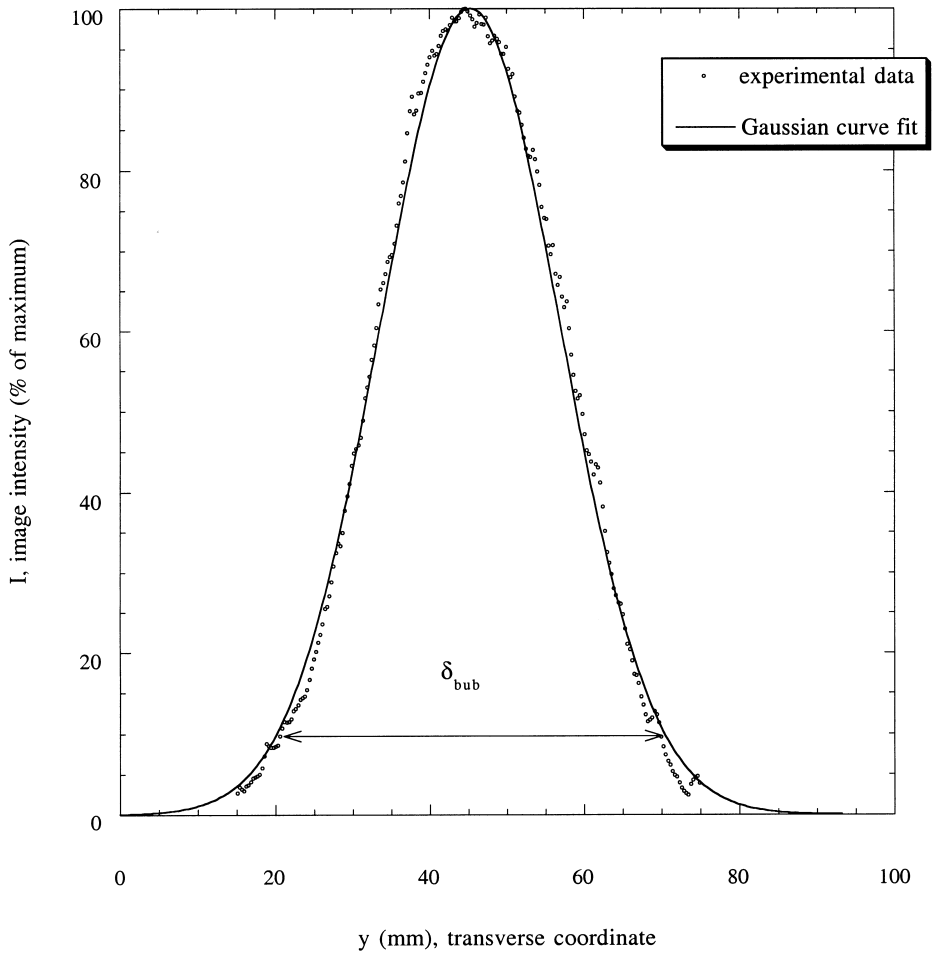

Fig. 4. Experimental and Gaussian bubble concentration distributions for the 2.5 mm bubbles in the low-speed turbulent shear layer for the most upstream portion of the field of view.

To compute the non-dimensional diffusion parameters (local Stokes number, eddy Froude number, and relative turbulent intensity) at each test condition requires estimates of turbulent intensity and length scale in the current planar free shear layer. The average v'_{rms} across the shear layer was approximated as $c_1\Delta u$, where Δu is the streamwise velocity difference across the shear layer and c_1 is an empirical constant, taken as 0.07 from Loth (1997). Similarly, the average Λ across the shear layer was approximated as $c_2\delta_{vel}$ where c_2 is an empirical constant, taken as 0.33 from Loth (1997). These empirical values are consistent with detailed measurements of Oakley et al. (1996) taken in this same turbulent shear layer facility. The values for the bubble terminal velocity and mean liquid velocity were obtained using Particle Image Velocimetry using the technique of Oakley et al. (1996). The Bond number was computed by assuming a surface tension of the air–water interface of 0.073 N/m.

3. Results

Fig. 5 shows the standard deviation of the experimental bubble concentration width versus streamwise distance for the three nominal bubble sizes at both flow speeds. For each condition, δ_{bub} grows approximately linearly with streamwise distance over the field of view, indicating that the bubble concentration width growth rate in this region is approximately linear as well (although it obviously spread much faster near the injector where average turbulence levels were highest). The results show that increasing the equivalent bubble diameter for the range of ellipsoidal bubbles studied consistently resulted in larger values of δ_{bub}. In addition, as the flow speed was increased for a given bubble size, δ_{bub} also showed a consistent increase.

The trend of increasing concentration width with increasing bubble diameter was independently verified by an earlier set of experiments which recorded individual trajectories of several bubbles at each nominal diameter (e.g. Fig. 6 for 3.5 mm diameter bubbles), using the method of Ford and Loth (1998). The rms of these individual transverse bubble positions (approximately forty positions for each case) relative to the injector position was computed to give a qualitative measure of bubble concentration width. The resulting transverse widths exhibited a similar quantitative increase as the equivalent bubble diameter increased (indeed these results were a motivation for this study). The qualitative trends of increasing thickness with increasing flow speed were also previously noted, and were in fact easily verified by simple visual observation (by eye) of the mean bubble distribution changes as flow speed was increased.

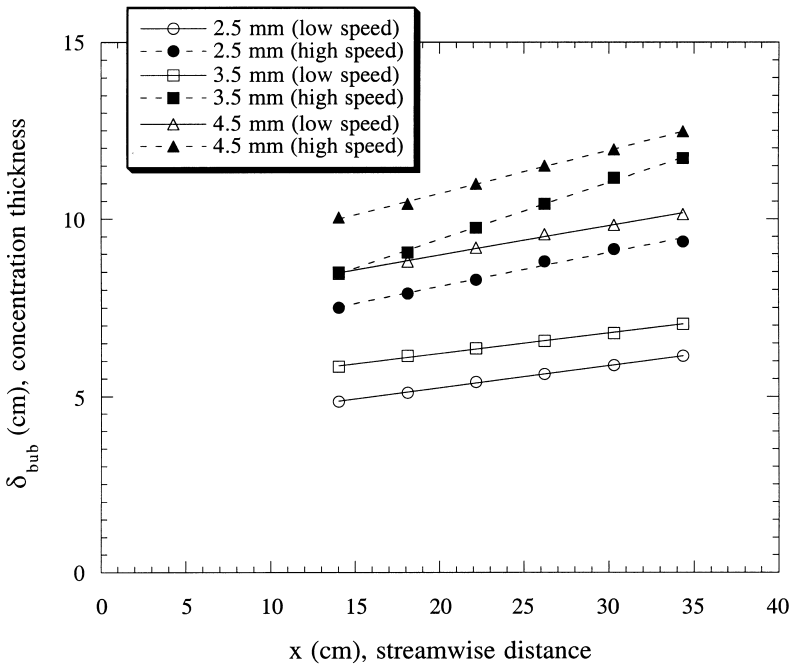

Fig. 5. Bubble concentration width versus streamwise coordinate (relative to injection position) for the three nominal bubble sizes and two flow speeds.

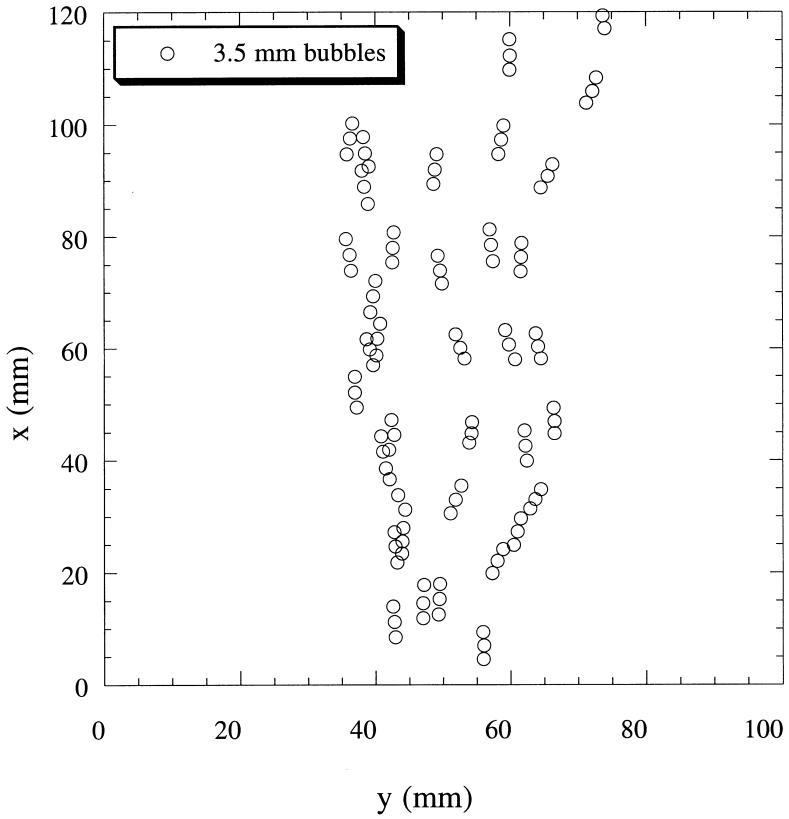

Fig. 6. Trajectories of the nominal 3.5 mm bubbles within the turbulent shear layer.

In order to better interpret the results in a temporal reference frame, experimental bubble concentration widths were extracted for the condition of equal bubble convection times for a given flow speed. This was accomplished by interpolating the data from Fig. 5 at different streamwise locations for each test condition. For this, an arbitrary scalar convection position of $x = 14$ cm was selected for both flow speed conditions such that the concentration width was extracted at streamwise positions equal to $[1 + V_{\text{term}}/u_{\text{mean}}] \times 14$ cm. The bubble

Table 1
Dimensional test conditions and results

d_B (mm)	V_{term} (cm/s)	Δu (cm/s)	u_{mean} (cm/s)	δ_{vel} (mm)	$\delta_{\text{bub,ref}}$ (mm)
2.47	27.0	0.33	26.0	80.0	57.7
3.64	32.1	0.33	26.0	80.0	68.6
4.42	37.0	0.33	26.0	80.0	101.4
2.27	23.6	0.60	65.0	84.0	80.9
3.27	27.1	0.60	65.0	84.0	93.9
3.67	32.4	0.60	65.0	84.0	111.1

concentration width obtained in this way is denoted as $\delta_{bub,ref}$ and as such is intended to approximately correct for mean drift bias (discussed in Section 1) and can thus be evaluated in terms of temporal diffusion (vs. spatial diffusion). The corrected concentration widths of the bubble distributions ($\delta_{bub,ref}$) are shown in Table 1 for the range of bubble diameters and flow speeds tested. (Note, the high speed condition resulted in slightly smaller bubbles for each nominal bubble size.) Again, we note an increasing concentration width as bubble diameter and flow speed increase, although the latter trend is not as exaggerated as that found for the uncorrected widths shown in Fig. 5.

To help explain, the individual causes of the two trends for concentration width noted in Table 1 (an increase with bubble size and an increase with flow-speed), the test conditions and results are considered in non-dimensional form, as given in Table 2. For the first trend of increasing width as bubble diameter increases, we note that the significant increase in bubble concentration width for a constant flow speed (constant Froude number) is associated with a modest increase in Stokes number and a corresponding modest decrease in relative turbulent intensity. Based on theoretical results from Loth (1997) for non-deformable bubbles, such small variations in St_Λ or ζ are expected to yield an insignificant variation in spatial diffusion rates and if anything would be associated with decreased turbulent diffusion. As such, the three turbulent diffusion parameters used to classify non-deformable diffusion are deemed to be approximately constant (for a given flow speed) and inappropriate to describe this trend of increasing diffusion with bubble diameter (which is also illustrated in Fig. 7 for constant Froude numbers). However, the significant increases in Bond number (with increasing bubble size) are known to result in increases in both bubble deformability and associated transverse oscillations in quiescent flow. Increases in such transverse oscillations for a relative reference frame have also been found in turbulent flow (Ford and Loth, 1998). Therefore, it is reasonable to assume that the increase in deformation-induced oscillations is directly related to and thus responsible for the increase in bubble concentration widths as diameter increases. However, it should be noted that for a given bubble diameter, the level of bubble diffusion was much less for the quiescent case than for the present turbulent flow cases. As such there is an important interplay between the turbulent flow and the deformation-induced oscillations that leads to the overall trend shown in Fig. 7. One might expect that such a relationship between Bond number and overall diffusion may be reduced in strength as the relative turbulent intensity ratio is increased. However, this reduction is not necessarily confirmed by the Fig. 7

Table 2
Non-dimensional test conditions and results

St_Λ	Fr_Λ	u_{mean}/V_{term}	ζ	B	$\delta_{bub,ref}/\delta_{vel}$
0.0118	0.034	0.096	0.085	0.8	0.72
0.0122	0.034	0.81	0.071	1.8	0.86
0.0144	0.034	0.70	0.062	2.6	1.27
0.0196	0.109	2.75	0.179	0.7	0.96
0.0206	0.109	2.40	0.156	1.4	1.12
0.0217	0.109	2.01	0.130	1.8	1.32

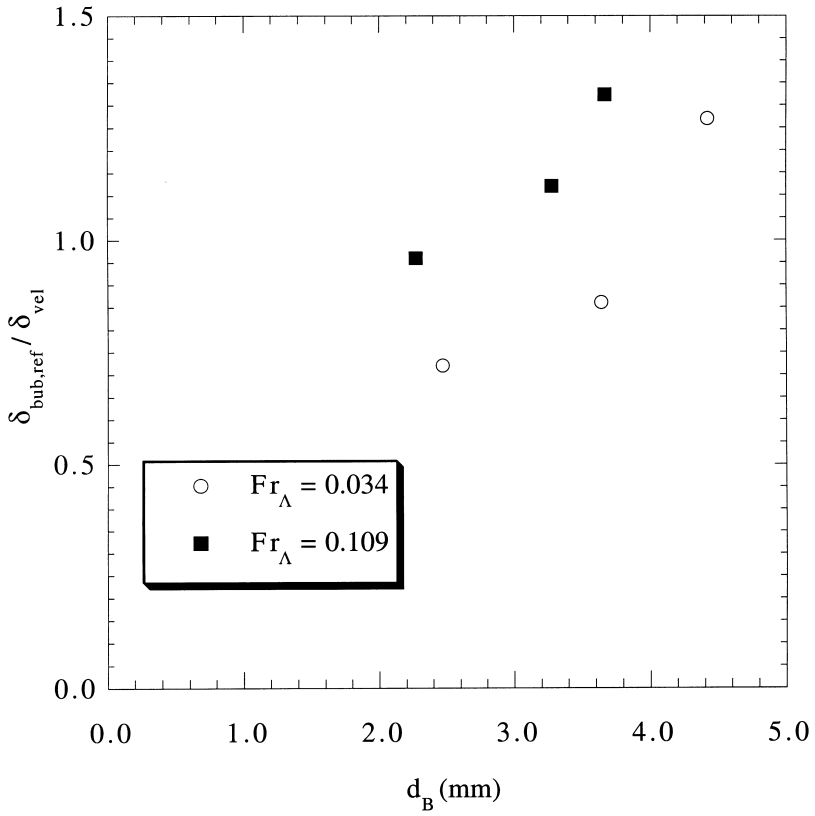

Fig. 7. Non-dimensional bubble concentration width versus bubble diameter for the two Froude numbers.

results when the increases with Bond number are compared at the two different Froude numbers.

Now let us consider the second trend, i.e. the increase of $\delta_{bub,ref}$ due to increased flow speed. In contrast to the first trend, this is associated with significant increases in all three of the non-dimensional turbulence parameters (St_Λ, Fr_Λ, ζ) for an approximately constant Bond number (bubble size) as shown in Fig. 7. Since we do not have independent variation of the three parameters it is difficult to say which one is primarily responsible for the increase in bubble concentration width. In order to simplify the discussion, we will examine only the influence of St_Λ and ζ since two of the three parameters can be considered independent. We first note that even for a 60% increase in Stokes number (as typically found between the two flow speeds for constant Bond number), the resulting changes in diffusion are expected to be modest (Loth, 1997). In addition, such an influence would be if anything to reduce the diffusion at larger Stokes number. But this is inconsistent with the results shown in Table 2. As such, St_Λ is not expected to be responsible for the increase in concentration width. Considering the other parameter, we note the ratio of eddy-interaction time to eddy-lifetime is approximately $\zeta/(\zeta+1)$, once the crossing trajectory effect is considered. As such, an increase in ζ corresponds to an increase in the eddy interaction time for a given eddy-lifetime, which in turn

would be expected to yield increased diffusion for a given bubble size (Loth, 1997). Such a trend is consistent with the results shown in Table 2 and Fig. 7. However, it is not clear whether the increases in $\delta_{bub,ref}$ would be even greater if the Stokes number would have been held constant. Therefore more test results are needed to confirm the quantitative effects of the various non-dimensional parameters.

5. Conclusions

A photographic technique was used to record transverse concentration distributions of ellipsoidal air bubbles in a two-stream, turbulent planar free shear layer of tap water. The void fraction was very low such that the turbulence was not significantly affected by the presence of the bubbles. From the digitized image intensity distributions, the Gaussian dispersion widths of the bubble concentration distribution were measured for three bubble sizes, two shear layer speeds, and six streamwise locations. For all conditions, the width of the bubble concentration distribution grew approximately linearly over the field of view. A correction was made to account for the mean drift bias in order to examine the temporal diffusion trends governing the concentration thickness. An increase in bubble concentration thickness was consistently noted for both an increase in bubble diameter (at a constant flow speed) and an increase in flow speed (at constant bubble diameter). These two trends were individually considered with respect to the characterizing non-dimensional parameters. The first trend was attributed to an interplay of turbulent diffusion with increasing deformation-induced trajectory oscillations (which result from larger bubble sizes and accordingly larger Bond numbers). The second trend was attributed to the increase in relative turbulence intensity, which allowed for longer bubble-eddy interaction times and thus increased turbulent diffusion. However, more work is necessary to understand the individual influence of the Stokes number on the spread of ellipsoidal bubbles.

Acknowledgements

This work was supported by the Office of Naval Research (ONR) under contracts N00014-95-1-0313 and N00014-96-1-0312 with Dr. Edwin Rood as technical monitor.

References

Clift, R., Grace, J.R., Weber, M.E., 1978. Bubbles, Drops, and Particles. Academic Press, New York.

Elgobashi, S., 1994. On predicting particle-laden turbulent flows. Applied Scientific Research 52, 309–329.

Ford, B., 1997. Dynamics of ellipsoidal bubbles in a turbulent shear layer. M.S. thesis, University of Illinois at Urbana-Champaign, Urbana, IL.

Ford, B., Loth, E., 1998. Forces on ellipsoidal bubbles in a turbulent shear layer. Physics of Fluids 10 (1), 178–188.

Loth, E., 1997. Turbulent dispersion model for heavy or buoyant particles in a turbulent free shear flow. ASME Fluids Engineering Division Summer Meeting, Vancouver, BC, FEDSM97-3607.

Loth, E., Cebrzynski, M.S., 1995. Modulation of shear layer thickness due to large bubbles. Int. Journal of Multiphase Flow 21 (56), 919–927.

Oakley, T., Loth, E., Adrian, R., 1996. Cinematic particle image velocimetry of a turbulent free shear layer. AIAA Journal 34 (2), 299–308.

Sene, K.J., Hunt, J.C.R., Thomas, N.H., 1994. The role of coherent structures in bubble transport by turbulent flows. Journal of Fluid Mechanics 259, 219–240.

Serizawa, A., Kataoka, I., Michiyoshi, I., 1975. Turbulence structure of air–water bubbly flow. Part III: Transport properties. Int. Journal of Multiphase Flow 2, 247–259.

Stewart, C.W., Crowe, C.T., 1993. Bubble dispersion in free shear flows. Int. Journal of Multiphase Flow 19 (3), 501–507.

Stock, D.E., 1996. Particle dispersion in flowing gases — 1994 Freeman scholar lecture. Journal of Fluids Engineering 118 (1), 4–17.

Tio, K., Lasheras, J., Ganan-Calvo, A., Linan, A., 1993. The dynamics of bubbles in periodic vortex flows. Journal of Applied Scientific Research 51, 285–290.